

RESEARCH PAPER

CHARACTERIZATION OF HOT DEFORMATION BEHAVIOR FOR ULTRA-HIGH STRENGTH STEEL CONTAINING TUNGSTEN

Taher El-Bitar¹, Maha El-Meligy^{1*}, Wojciech Borek², Saad Ebied³

¹ Plastic Deformation Dept., Central Metallurgical R&D Institute (CMRDI), 1st Elfelazaat St., Eltebeen, 11722 Helwan, Egypt

² Engineering and Biomedical Materials Depart., Faculty of Mechanical Technology- Silesian University of Technology, Ul. Konarskiego 18a, 44-100 Gliwice, Poland

³ Production Engineering and Mechanical Design Department, Faculty of Engineering - Tanta University, Tanta 31527, Egypt

*Corresponding author: dr.mahaelmeligy@gmail.com, tel.: +201002268662, Plastic Deformation Dept., Central Metallurgical R&D Institute (CMRDI), 1st Elfelazaat St., Eltebeen, 11722 Helwan, Egypt

Received: 04.06.2023

Accepted: 31.07.2023

ABSTRACT

The steel alloy of the current study contains 0.3% carbon with different amounts of Cr, and Mo, in addition to W. Single simulation hits were designed as isothermal passes for compressive hot deformation up to 0.5 true strain. Each simulation compressive pass was carried out at temperatures, 1050, 950, 850 and 750 °C, with strain rates 0.1 and 1.0 sec⁻¹. A numerical computational model is used for formulation of the alloy hot flow behavior at the specified conditions. The model considers inseparable strain hardening mechanism and dynamic softening phenomenon. It is noticed that high deformation temperature lowers the flow stress value (σ_f), while the increase of the strain rate raises it. The flow curves reveal initial high strain hardening phenomena in combination with low dynamic softening features. With the increase of strain, the dynamic softening, becomes dominant, and the flow stress gradually drops until a relatively stable stress level. Predicted flow curves were then constructed and compared with their counterpart experimental flow curves. The predicted flow curves are typically matching the counterpart experimental ones.

Keywords: Hot Deformation behavior; Ultra-High Strength Steel; Computational flow curve model; Strain hardening; Dynamic softening; Isothermal flow curves; Dynamic recovery; Recrystallization

INTRODUCTION

Ultra high strength steels (UHSS) are being continuously explored to meet the growing demand of advanced industries [1]. UHS steels have emerged as the most promising candidate material for dynamic energy penetrators, due to their excellent high strength and hardness as well as good toughness [2]. However, the practical application is still limited due to poor processing performance, high deformation resistance, and complex heat treatment process parameters [3].

Nevertheless, the hot-forming process significantly depends on the nonlinear relationship between the microstructural evolution and deformation parameters [4, 5]. Moreover, different metallurgical mechanisms, such as strain hardening, dynamic softening, and dynamic recrystallization (DRX), are affected by the deformation conditions [6]. Thermo-mechanical simulation is used to achieve the hot deformation behavior for precise control of hot deformation parameters that obtain the desired mechanical properties of UHSS components [7].

Usually, an accurate constitutive model is a prerequisite for the numerical simulation of plastic flow behavior during hot forming processes [8]. Hot compressive behavior of GH4698 superalloy was examined in the temperature range of 950–1100 °C and strain rate range of 0.001–1.0 sec⁻¹[8]. Observations on the

flow curves reveal strain hardening and dynamic recovery features at the beginning of the deformation, leading to a rapid increase of the flow stress. After exceeding a peak level of the flow stress, the dynamic softening was enhanced by dynamic recrystallization (DRX) and the flow stress gradually drops until a relatively stable stress level [8]. On some other study of the deformation behavior of plain carbon steel, [9], three types of dynamic recrystallization (DRX) were identified, namely single peak, multiple transient steady state (MTSS), and cyclic behaviors. Isothermal compression tests were carried out to predict the hot deformation behavior of Al-3%Mg2Si in the temperature range of 300–500 °C and strain rate range of 0.01–5 sec⁻¹ [10]. The flow stress curves reveal a typical dynamic recovery characteristic. A modified Arrhenius-type constitutive equation was built to describe the flow behavior of Al-3% Mg2Si alloy [10] and, flow behavior of high-Cr ultra-super-critical rotor steel [11]. Flow stresses of grade 300M steel were corrected to eliminate the effects of both adiabatic heating and friction during hot compression [12]. Based on the corrected flow stress curves, a modified constitutive model was established to quantify the flow behaviors accurately [12].

The constitutive equations models would comprise effects of the metallurgical mechanisms, to support the simulation of the hot

forming behavior [13]. Three of the constitutive models have been widely applied to explore the hot deformation behavior of different alloys. These constitutive models are including the Arrhenius model [14], Johnson-Cook (JC) model [15], and Halal and Kaftanoglu model, [16]. Despite the convenience and universality of the empirical models, their biggest drawback is the lack of physical significance. Therefore, it is imperative to further optimize the constitutive model to describe accurately the deformation mechanisms features.

In the current work, isothermal single hits were carried out with the aid of the thermo-mechanical simulator (Gleeble 3800) for prediction of the hot deformation behavior during hot forging process of UHSS alloy containing W at specific temperatures and strain rates. The model proposed by Halal and Kaftanoglu [16], is being considered throughout the current investigation for prediction of the hot deformation behavior of the current UHSS alloy.

MATERIAL AND METHODS

Experimental Procedure

The steel alloy under investigation was processed at the experimental foundry shop in CMRDI of Egypt. The alloy is designed as ultra-high strength (UHS) martensitic steel containing mainly about 0.3% carbon in addition to 2.48% Cr, 0.29% Mo, 0.9% Ni and 1.63% W. The alloy was cast as Y-shape ingots with effective ingot dimensions 300x200x35 mm.

XRD investigation was used to identify the existing phases and compounds in the current alloy at the forged state. The critical and allotropic transformation temperatures were evaluated by using the commercial software package “J-Mat pro”. An optical microstructure of cross sectional specimens from forged bars was also done to identify the hot forged existing phases.

Representative specimens were taken from the forged round bars for machining to cylindrical shapes with dimensions 8.0 mm diameter and 11.0 mm height to suite the hot compressive investigation at the thermo-mechanical simulator (Gleeble 3800) for isothermal single hits to explore the alloy flow behavior under controlled hot deformation conditions.

The carbide end of the simulator is provided with a set of graphite and tantalum foils 0.1 mm thick to reduce the friction between the specimen's surface and the anvils. The simulator testing-chamber was air-evacuated to 3×10^{-1} mbar. Argon gas was then introduced to the testing chamber at 200 m.bar pressure where the tests were performed in an argon atmosphere. Fig. 1-a presents schematically the isothermal compressive single hits, while Fig 1-b shows hot deformation cycle carried by using the thermo-mechanical simulator (Gleeble 3800).

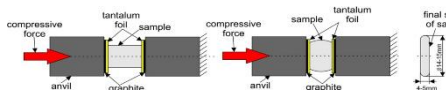


Fig. 1-a Graphical presentation of the compressive single hits by using the thermo-mechanical simulator (Gleeble 3800)

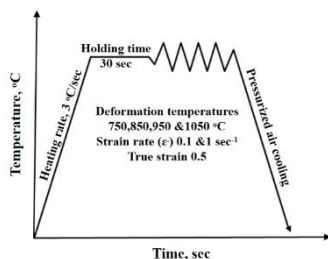


Fig. 1-b Schematic presentation of isothermal hot deformation cycle

The single hits specimens were heated at a rate of 3 °C/sec up to the predetermined deformation temperatures, 1050, 950, 850 and 750 °C and soaked for 30 sec. to homogenize the temperature throughout the entire sample. The deformation rates were adapted at 0.1 and 1.0 sec⁻¹. Finally, the samples were compressed to 0.5 true strain. Soon after testing, the samples were cooled to the room temperature with pressurized air.

The simulator generates massive experimental data of compressive force, displacement, time and temperature for each single hit at specific testing conditions. True stress-true strain and strain rate at a specific temperature are computed and flow curves are then delivered. The A.S.Halal and D. Kaftanoglu computational model [16] was used throughout the current investigation to characterize the hot deformation behavior of the steel alloy.

The model [16] was represented by the following polynomial stated in equation (1);

$$\sigma_f = [\gamma_0 * (1 + B\phi)^n] + [-A * (\phi)^m] \quad (1)$$

Where; σ_f & ϕ are flow stress and true strain respectively, while γ_0 , B, n, A, and m are material constants and test conditions.

The material constants and test conditions were predicted based on the massive experimental data, which were generated by the thermo-mechanical simulator (Gleeble 3800).

It is worth to notice that the model considers two inseparable mechanisms at a specific strain rate and test temperature. i.e. a strain hardening mechanism is accompanied by a dynamic softening phenomenon. Fig. 2 presents the strain hardening and dynamic softening effects separately and assembled as presented by the model in Eq. (1).

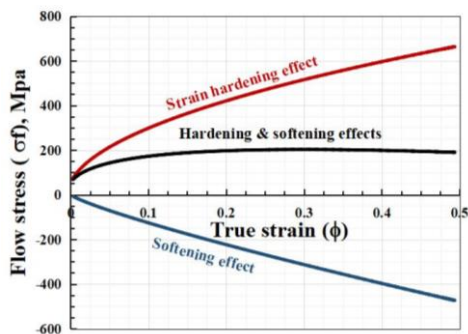


Fig. 2 Strain hardening and dynamic softening effects separately and assembled

The model secures initial flow stress value even at zero strain, while softening sits at zero level. Strain hardening and dynamic softening effects increase continuously with the increase of strain. Fig. 2 shows that deformation starts with initial high strain hardening accompanied with low dynamic softening, where the strain hardening is playing a leading role. By increasing strain, the flow stress rises continuously reaching to a balance with a dynamic softening effect, which is working against the strain hardening effect and forming a plateau deformation behavior.

RESULT AND DISCUSSION

The chemical composition of the steel alloy under investigation is a good sign that the alloy contains mostly martensitic constitute.

Fig. 3 presents XRD phase-intensity chart of the steel alloy under investigation. The chart confirms that the alloy contains martensite phase, tungsten carbides and few of retained austenite, combined with each other.

Fig. 4 presents an optical microstructure, at a magnification 100X, for a cross-sectional hot forged specimen. The micro graph clearly ensues a fine lath martensite matrix in combination with elongated white regions. These regions are occupied by remnant carbides of the alloying elements in addition to a retained austenite phase (RA), as previously confirmed by the XRD chart in **Fig. 3**. The micro graph presented by **Fig. 4** contains fine lath martensite colonies arranged parallel to the forging direction, while the elongated white regions are surrounding the outside borders of the martensite colonies [17].

The microstructure has a pronounced effect on the flow curve behavior of the alloy, while the test temperature is more effective on controlling the value of flow stress [18]. The Ac1 and Ac3 critical transformation temperatures were valuated, by using "J-Mat pro software", as 774 and 796 °C respectively.

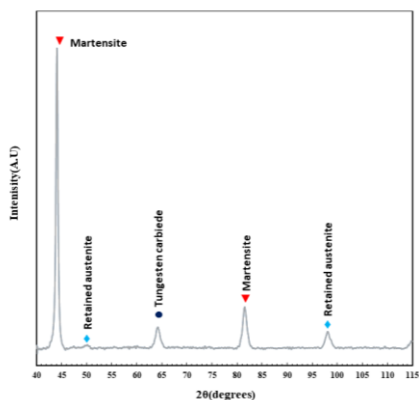


Fig. 3 XRD phase-intensity chart of the steel alloy

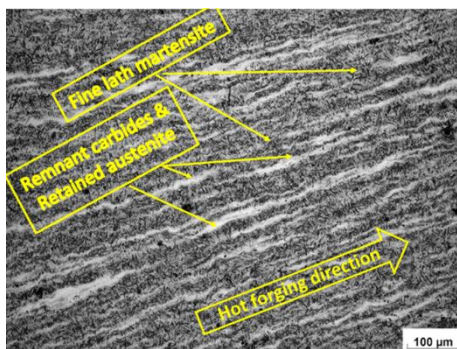


Fig. 4 Fine lath martensite matrix with white regions occupied by remnant carbides of the alloying elements and retained austenite (RA) phase

Fig. 5 presents the isothermal flow curves of the alloy under investigation at temperatures 1050, 950, 850 and 750 °C. The strain rate is varied as 0.1 and 1.0 sec⁻¹. It is found that the increase of the strain rate raises the value of flow stress (σf) to be higher than that at a lower strain rate at the same test temperature. The flow stress of the hot deformed alloy is mainly controlled by dislocation climb during their intragranular motion

[9]. At low strain rate, (0.1 sec⁻¹) the dislocations have a chance for easy glide and piling up to pass over the intragranular, while at a higher strain rate (1.0 sec⁻¹), there is a less time for piling up against the intragranular and obstacles to climb and pass over them. Consequently, the alloy possesses higher resistance for individual dislocations to climb and pass over the obstacles showing higher flow stress.

Furthermore, the flow curves at temperatures 1050, 950, and 850 °C are considered as an ideal flow behavior, where the alloy possesses austenitic microstructure (at a temperature >Ac3). Usually, flow curves serration at high strain rates (1.0 sec⁻¹) manifests due to less time for dislocation to pile up climb during deformation.

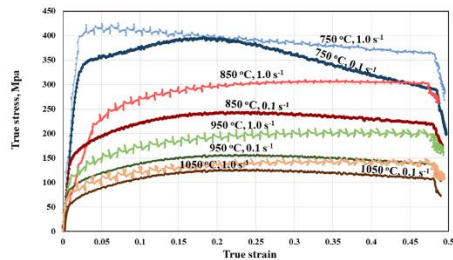


Fig. 5 Flow curves behavior of isothermal single compression hits at temperatures 1050, 950, 850 and 750 °C, for strain rates 0.1 and 1.0 sec⁻¹

Observations on the flow curves in **Fig. 5** reveal initial high strain hardening and low dynamic softening features at the beginning of the deformation, leading to a rapid increase of the flow stress (σf). By increasing the true strain to about 0.2, the dynamic softening, which is enhanced by dynamic recovery becomes dominant, and the flow stress gradually drops until a relatively stable stress level [8].

However, flow curves of the alloy at 750 °C (lower than Ac1) behaves different, where microstructure of critical transformations happens. Low test temperature is leading to a high value of the Z-parameter [19], which would enhance and accelerate dynamic softening. At low strain rate (0.1 sec⁻¹), a peak stress value is pronounced on the flow curve at 0.2 true strain, announcing creation of dynamic softening phenomenon and the flow stress becomes further declined. Furthermore, at higher strain rate (1.0 sec⁻¹), the Z-parameter becomes exaggerated, which is leading to an early peak stress at 0.05 true strain, followed directly by inclined downstream behavior of the flow curve, ensuring creation of dynamic recrystallization phenomena [20].

The excessive data of the flow curves are used for numerical valuation of the material constants and test conditions of the flow curves on the bases of the proposed computational model [16]. The numerical values of material constants (yo, B, n, A and m) and test conditions (test temperature, strain rate) are stated in **Table 1**.

Table 1 Numerical values of material constants and test conditions of the flow curves

Temp.	Strain rate	yo	B	n	A	m
1050	0.1	30	200	0.59	700	0.98
	1	32	200	0.59	700	0.98
950	0.1	48	265	0.51	800	0.83
	1	55	265	0.51	850	0.83
850	0.1	82	560	0.43	1107	0.65
	1	85	580	0.43	1050	0.65
750	0.1	193	590	0.327	1500	0.64
	1	195	590	0.3	1180	0.67

Predicted flow curves were constructed at temperatures 1050, 950, 850 and 750 °C with strain rates 0.1 and 1.0 sec⁻¹ using the corresponding values presented in Table 1. The predicted curves are compared with their counterpart experimental flow curves in Fig. 6. It is found that the predicted curves are typically matching the counterpart experimental flow curves.

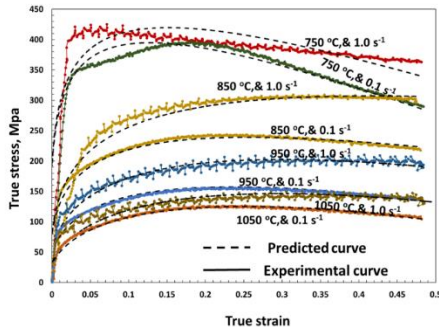


Fig. 6 Experimental flow curves compared with the predicted ones at temperatures 1050, 950, 850 and 750 °C for strain rates 0.1 sec⁻¹ and 1.0 sec⁻¹

CONCLUSIONS

1. Microstructure of the forged steel alloy contains fine lath martensite matrix in combination with regions occupied by remnant carbides of the alloying elements in addition to a retained austenite phase (RA).
2. The proposed numerical computational model considers two inseparable mechanisms (strain hardening and dynamic softening) during hot deformation.
3. High deformation temperature lowers the flow stress value (σ_f), while the increase of the strain rate raises it.
4. The flow curves reveal initial high strain hardening phenomena in collaboration with low dynamic softening features. With the increase of strain, the dynamic softening, becomes dominant, and the flow stress gradually drops until a relatively stable stress level.
5. Flow curves at temperature 750 °C (<Ac₁) show hardening mechanism, dynamic recovery followed by a peak stress and dynamic recrystallization phenomena.
6. Predicted flow curves were constructed and compared with their counterpart experimental ones. The predicted flow curves are typically matching the counterpart experimental ones.

Acknowledgments: Authors are grateful for administration board of CMRDI, who accepted and permitted the financial support for the project. Further thankful to the technical & experimental support of CMRDI.

REFERENCES

1. J. Li, D. Zhan, Z. Jiang, H. Zhang, Y. Yang, Y. Zhang: Journal of Materials Research and Technology, 23, 2023, 172-190. <https://doi.org/10.1016/j.jmrt.2022.12.177>.
2. R.D Conner, R.B. Dandliker, V Scruggs, W.L Johnson: International Journal of Impact Engineering, 24(5), 2000, 435-444. [https://doi.org/10.1016/S0734-743X\(99\)00176-1](https://doi.org/10.1016/S0734-743X(99)00176-1).
3. Q. Wang, J. Shi, J. Cai, Y. Feng: High Temperature Materials and Processes, 38, 2019, 452-460. <https://doi.org/10.1515/htmp-2018-0042>.
4. V. Rielli, F. Godor, C. Gruber, A. Stanojevic, B. Oberwinkler, S. Primig: Materials and Design, 212, 2021, 110295. <https://doi.org/10.1016/j.matdes.2021.110295>.

5. Z. Ma, G. Li, Z. Su, G. Wei, Y. Huang, N. Hort, A. Hadadzadeh, M. A. Wells: Journal of Materials Research and Technology, 19, 2022, 3536-3545. <https://doi.org/10.1016/j.jmrt.2022.06.047>.
6. X. Chen, Y. Lin, D. Wen, J. Zhang, M. He: Materials & Design, 57, 2014 568-577. <https://doi.org/10.1016/j.matdes.2013.12.072>.
7. T. El-Bitar, M. El-Meligy, E. El-Shenawy, A. Almosilhy, N. Dawood: International Journal of Chemical, Molecular, Nuclear, Materials and Metallurgical Engineering, 11(3), 2017, 179-185.
8. X. M. Chen, M.T. Ning, H.W. Hu, Y.C. Lin, X.J. Zhou, J. Zhang, X.Z. Lu, J. Chen, Y.X. Liu: Materials Characterization, 201, 2023, 112916. <https://doi.org/10.1016/j.matchar.2023.112916>.
9. S. Saadatkia, H. Mirzadeh, J. M. Cabrera: Materials Science and Engineering: A, 636, 2015, 196-202. <https://doi.org/10.1016/j.msea.2015.03.104>.
10. M. Hu, Y. Sun, J. He, C. Li: Materials Characterization, 183, 2022, 111623. <https://doi.org/10.1016/j.matchar.2021.111623>.
11. Z. Y. Ding, Q. d. Hu, L. Zeng, J. Guo: International Journal of Minerals, Metallurgy and Materials, 23(11), 2016, 1275-1285. <https://doi.org/10.1007/s12613-016-1349-2>.
12. M. Zhao, L. Huang, C. Li, J. Li, P. Li: Materials Science and Engineering: A, 810, 2021, 141031. <https://doi.org/10.1016/j.msea.2021.141031>.
13. Y. Lu, H. Xie, J. Wang, Z. Li, F. Lin, J. Han, J. Han, Z. Jiang: Vacuum, 186, 2021, 110066. <https://doi.org/10.1016/j.vacuum.2021.110066>.
14. X. Q. Yin, S. W. Lee, Y. F. Li, C. H. Park, X. J. Mi, J. T. Yeom: Metals and Materials International, 23(5), 2017, 1002-1011. <https://doi.org/10.1007/s12540-017-6736-3>.
15. X. M. Chen, Y. C. Lin, H. W. Hu, H. C. Luo, X. J. Zhou, Y. Huang: Advanced Engineering Materials, 23(1), 2020, 2000704. <https://doi.org/10.1002/adem.202000704>.
16. A. S. Halal, D. Kaftanoglu: Computer-Aided Modeling of Hot and Cold Rolling of Flat Strip: Int. Conf. on Computers in Engineering, Las Vegas, Nevada, 1984.
17. L. Zhong, B. Wang, C. Hu, J. Zhang, Y. Yao: Metals, 11(8), 2021, 1239. <https://doi.org/10.3390/met11081239>.
18. M El-Meligy, T El-Bitar: Procedia Manufacturing 50, 2020, 771-776. <https://doi.org/10.1016/j.promfg.2020.08.139>.
19. T. El-Bitar, M. El-Meligy, M. Kheir: Procedia Manufacturing, 50, 2020, 173-178. <https://doi.org/10.1016/j.promfg.2020.08.032>.
20. T. O. Webb, D. C. Van Aken, S. N. Lekakh: Evaluating Chemical Homogeneity in the Performance of Eglin Steel: 118th Annual Metal casting Congress, Schaumburg, Illinois, 2014.